

Cargo-dependent mode of uptake and bioavailability of TAT-containing proteins and peptides in living cells

Gisela Tünnemann,* Robert M. Martin,* Simone Haupt,[†] Christoph Patsch,[†] Frank Edenhofer,[†] and M. Cristina Cardoso*¹

*Max Delbrück Center for Molecular Medicine, Berlin, Germany; and [†]Institute of Reconstructive Neurobiology, Stem Cell Engineering Group, University of Bonn-Life and Brain Center and Hertie Foundation, Bonn, Germany

ABSTRACT Cell-penetrating peptides (CPPs) are capable of introducing a wide range of cargoes into living cells. Descriptions of the internalization process vary from energy-independent cell penetration of membranes to endocytic uptake. To elucidate whether the mechanism of entry of CPP constructs might be influenced by the properties of the cargo, we used time lapse confocal microscopy analysis of living mammalian cells to directly compare the uptake of the well-studied CPP TAT fused to a protein (>50 amino acids) or peptide (<50 amino acids) cargo. We also analyzed various constructs for their subcellular distribution and mobility after the internalization event. TAT fusion proteins were taken up largely into cytoplasmic vesicles whereas peptides fused to TAT entered the cell in a rapid manner that was dependent on membrane potential. Despite their accumulation in the nucleolus, photobleaching of TAT fusion peptides revealed their mobility. The bioavailability of internalized TAT peptides was tested and confirmed by the strong inhibitory effect on cell cycle progression of two TAT fusion peptides derived from the tumor suppressor p21^{WAF/Cip} and DNA Ligase I measured in living cells.—Tünnemann, G., Martin, R. M., Haupt, S., Patsch, C., Edenhofer, F., Cardoso, M. C. Cargo-dependent mode of uptake and bioavailability of TAT-containing proteins and peptides in living cells. *FASEB J.* 20, 1775–1784 (2006)

Key Words: cell-penetrating peptide • protein transduction • PCNA • PBD • Cre recombinase

THE PHENOMENON OF transduction denotes the size-independent *in vivo* delivery of a wide variety of cargoes into cells and is mediated by cell-penetrating peptides (CPPs). Although the internalization of fluorophores, nucleotides, peptides, globular proteins, nanoparticles, lipids, and drugs interconnected to CPPs into living cells has been described in the literature and resulted in measurable biological effects (1), the reported transduction experiments need to be critically evaluated in terms of the invasiveness of the detection methods utilized (2). Most known CPPs are parts of viral proteins or artificial derivatives thereof, and include several

arginines and/or lysines (reviewed in ref. 3). One of the best-studied CPP is a basic amino acid peptide from the transactivator of transcription (TAT) protein of the HIV-1 with the minimal transduction domain comprising amino acids 48–57 (4). The initializing step in the mechanism of cellular entry of CPPs is thought to be the strong ionic interaction between the positively charged amino acid residues and negatively charged plasma membrane constituents (5–7). Among the cationic groups mediating cellular uptake, the guanidinium group of arginine has been shown to be the most effective (8–10). Subsequent events needed for the internalization, however, differ between reports and are often conflicting. The first mechanistic studies led to the proposal that CPP internalization occurs rapidly in a receptor- and energy-independent manner (6, 9, 11–13) perhaps by destabilizing the lipid bilayer or by the formation of inverted micelles with subsequent release of their contents within the intracellular space (reviewed in ref. 14). More recently, an active mechanism based on vesicular uptake has been proposed as the general mode of internalization of CPP constructs into cells (15–19).

To understand whether the mechanism of entry is dependent on the cargo connected to the CPP, we directly compared TAT fused to globular proteins and TAT-containing peptides with respect to their uptake kinetics and their intracellular distribution after internalization in living cells. Transduced constructs were also analyzed for their ability to reach their targets inside the cell and to exert their biological activity.

MATERIALS AND METHODS

Peptides and proteins

Peptides (complete description in **Table 1**) were synthesized by Biosyntan GmbH (Berlin, Germany), Peptide Specialty Laboratories (Heidelberg, Germany), and Bachem (Weil am

¹Correspondence: Max Delbrück Center for Molecular Medicine, Robert-Rössle-Str. 10, Berlin 13125, Germany. E-mail: cardoso@mdc-berlin.de
doi: 10.1096/fj.05-5523com

TABLE 1. List of peptides and their uptake efficiencies^a

Peptide and label	aa sequence	kDa	pI	Peptide concentration	Transduction efficiency	Transduction threshold
R-PTD ₄	YARAARQARA	1.13	11.71	10 μM	0%	400 μM
F(Ahx)-TAT	YGRKKRRQRRR	1.93	12.31	1 μM	90%	1 μM
R-TAT (ri)	rrrqrkkrg	1.81	13.3	1 μM	90%	1 μM
bt-NLS	SGYGPKKKRKVG	1.93	10.68	10 μM	0%	n.a.
Lig1-PBD-F	MQRDIMSFFQPTKEFKAKK	2.80	10.00	10 μM	0%	n.a.
R-TAT-HA2(ri)	rrrqrkkrg-gdimgewgneifgaigflg	3.24	11.71	10 μM	80%	0.1 μM
F(Ahx)-TAT-Control	YGRKKRRQRRR-TALDASALQTE	3.05	11.72	20 μM	70%	n.d.
R-TAT(ri)-p21-PBD	rrrqrkkrg-aaA-GRKRRQTSMTDFYHSKRRLIFSa	4.96	12.43	20 μM	90%	7.5 μM
TAT-Lig1-PBD-R	YGRKKRRQRRR-GGG-MQRSIMSFFQPTKEGKAKK	4.38	12.14	10 μM	80%	5 μM

^aR, TAMRA/rhodamine; F, FITC; Ahx, aminohexanoic acid; capital letters, L-amino acids; small letters, D-amino acids; ri, retro inverso; n.a., not applicable; n.d., not determined.

Rhein, Germany). The PCNA binding domain (PBD) peptide TAT-p21-PBD is derived from human p21^{WAF/Cip} (20) and the Lig1-PBD as well as TAT-Lig1-PBD from mouse DNA Ligase I (21, 22). The peptides were analyzed by HPLC a second time at the end of the experiments to assure their stability under the storage conditions. The pI of the peptides was calculated using the program ProtParam (<http://au.expasy.org/cgi-bin/protparam>). His-NLS-TAT-Cre-recombinase (TAT-Cre) protein was produced, purified (23), and labeled with Alexa Fluor 633 or rhodamine as described (24). BL21 (DE3) cells (Novagen, Madison, WI, USA) were used for production of His-PTD₄-PCNA. Bacterial cultures were grown at 37°C until early-mid log phase and expression was induced by addition of 1 mM IPTG. Cells were harvested 3 h after induction, lysed by lysozyme treatment and ultrasonification, and His-tagged protein purified to >95% purity from cell lysates by affinity chromatography using Talon resin material (BD Bioscience, Franklin Lakes, NJ, USA) according to the manufacturer's instructions. The purified protein was labeled with Atto 633 NHS ester (Fluka, St. Louis, MO, USA) in 0.1 M bicarbonate buffer pH 8.5, then further purified and rebuffered into PBS pH 7.4 over a G25-Sephadex column (Pharmacia, Cambridge, MA, USA). BL21 (DE3) CodonPlus-RIL cells (Novagen) were used to produce His-TAT-MK2 (MAPKAP kinase 2). Bacterial cultures were grown and induced as above, and harvested cells were disrupted by 2-fold homogenization at a 1000 bar with a SLM AMINCO FrenchPress (Spectronic Instruments, Leeds, UK). More than 98% pure protein was obtained from the lysates upon Talon affinity chromatography, as before (BD Bioscience). The purified protein was labeled with Cy5 NHS ester (Amersham Bioscience, Arlington Heights, IL, USA) in 0.1 M bicarbonate buffer pH 8.5, then further purified and rebuffered into PBS pH 7.4 over a G25-Sephadex column (Pharmacia). The Cy5-labeled streptavidin (Amersham) was incubated for 30 min prior to the experiments with NLS-biotin peptides at molar ratios of 1:1 for biotin and biotin binding sites at homotetrameric streptavidin. The streptavidin-coated Quantum dots 525 were obtained from Quantum dot Corp. (Hayward, CA, USA).

Cell culture

The C2C12 mouse myoblast cells and C2C12 mouse myoblasts stably transfected with GFP-PCNA as a fluorescent cell cycle marker were cultured as described (25, 26). Flp 3T3 mouse fibroblasts were from Invitrogen (Carlsbad, CA, USA). 3T3-FDR1.2 Cre reporter cells (27) were cultured in Dulbecco's modified Eagle medium (DMEM) containing 10% fetal calf serum (Life Technologies, Inc., Grand Island, NY, USA). For

live cell microscopy, cells were plated onto 4- or 8-well LabTek coverglass chambers (NalgeNunc, Rochester, NY, USA).

Transduction assays and inhibitor treatments

All peptide and protein transduction experiments, except for the Cre recombinase assay (see below), were performed exclusively with living cells plated on 4- or 8-well LabTek coverglass chambers using an objective heated to 37°C. For transduction experiments, the medium was removed and PBS with the different peptides or proteins was applied directly to the cells. After 10 min incubation, PBS was replaced with the growth medium. Usually uptake was studied continuously starting with the peptide application over a period of at least 2 h, followed by incubation of the cells at 37°C under humidified atmosphere until additional image collection. Transduction efficiencies of peptides were determined by counting the numbers of cells with or without nucleolar signals and internalization efficiencies of proteins by counting cells with or without intracellular vesicles directly on the fluorescence microscope in three fields of view, each containing ~50 cells, or by a similar analysis performed on low magnification overview images. Cell viability after peptide or protein application was monitored by their ability to undergo complete mitotic cell cycles and grow to confluency over a period of 24 to 48 h. Membrane integrity was ascertained by the Trypan blue exclusion assay. Cytochalasin D (Sigma, St. Louis, MO, USA) was dissolved to 10 mg/ml in DMSO and sodium azide (Sigma) to 10% (w/v) in ddH₂O. Both stock solutions were adjusted to 1×PBS at the indicated final concentrations (Fig. 2) before being applied to living cells. The potassium buffer (Fig. 2) corresponds to PBS with all sodium-containing compounds substituted for the equivalent potassium-containing analogues. C2C12 mouse myoblasts were preincubated for the indicated times (t in Fig. 2) with different inhibitors in PBS or the potassium buffer. The TAT-containing peptide and protein were applied directly to the cells and mixed gently. For the potassium phosphate buffer experiment, the protein was dialyzed against the potassium buffer prior to application. After 10 min the cells were washed twice and incubated for another 20–60 min (as annotated in the phase contrast images for each treatment) in DMEM medium, except for the potassium buffer treatment where the medium was replaced by potassium buffer. Transduction thresholds were determined by incubating C2C12 mouse myoblasts with CPP-containing peptides in medium at different concentrations ranging from 0.1 to 500 μM for 1 h. The lowest peptide concentration leading to accumulation

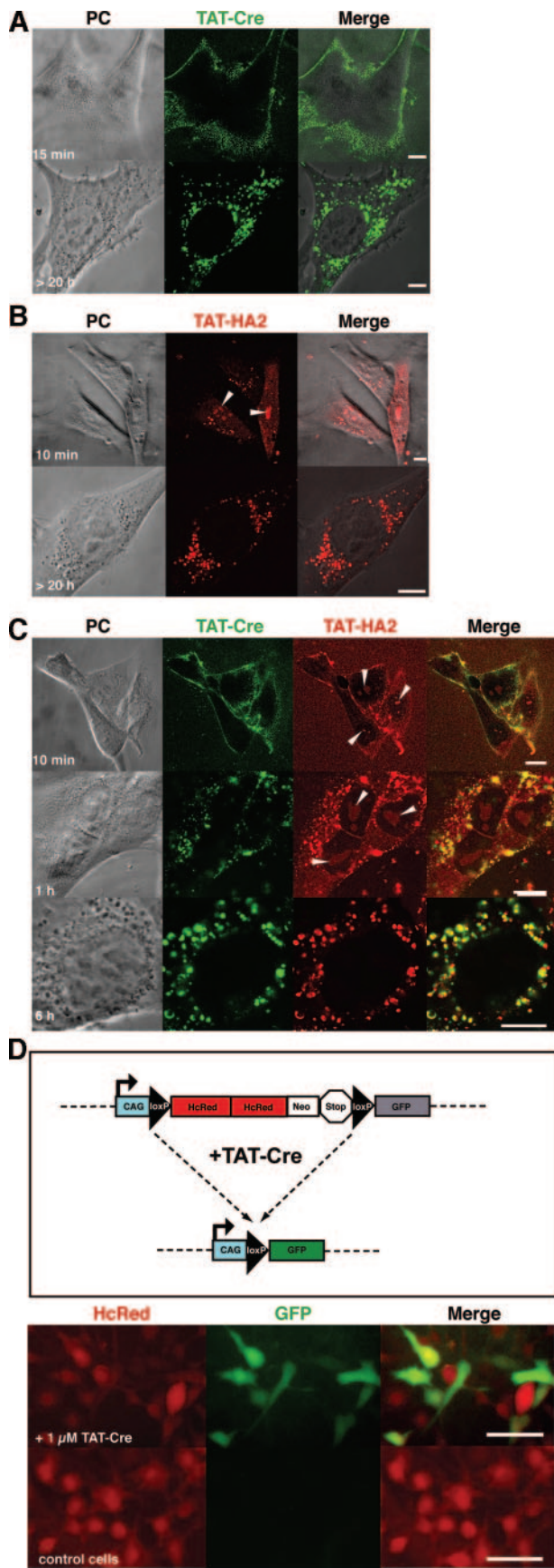


Figure 1. Differences in subcellular distribution of proteins and peptides fused to TAT after internalization in living cells. TAT-Cre and TAT-HA2 were applied to the cells for 10 min,

inside nucleoli was considered to be the transduction threshold from which transduction occurs.

Microinjection and bead loading

Intracellular delivery of the Lig1-PBD-F peptide was accomplished by bead loading using 100 μm silica beads. The beads were washed first in ethanol, then in growth medium, and finally pipetted onto the medium of cells grown in a self-made culture dish with a coverglass bottom. The Lig1-PBD-F solution was added subsequently and the chamber was shaken a few times. The beads were removed for microscopic observation of the labeled cells. Microinjection of the NLS-biotin peptide complexed with streptavidin-Cy5 was performed using an Eppendorf microinjection and micromanipulation system mounted on a Zeiss LSM510Meta inverted microscope setup. The parameters for cytoplasmic microinjection were set to 0.7 s injection time with 15 fPa injection pressure.

Cre recombinase double reporter assay

3T3-FDR1.2 cells (27) were cultured to 50% confluency in 6-well plates. The pFDR reporter gene construct allows detection of bioactive Cre recombinase by switching from constitutive HcRed to GFP expression (Fig. 1 D). For transduction, the cells were incubated with 2 μM TAT-Cre protein diluted into a 50:50 mixture of PBS and DMEM for 3 h, washed once with PBS, then cultivated in normal medium. Fluorescence microscopy was performed 24 h after transduction.

Live cell assay for cell cycle inhibition

C2C12 mouse myoblasts stably expressing GFP-PCNA (26) were synchronized by mitotic shake-off and plated onto 8-well LabTek coverglass chambers. After becoming adherent, the number of cells that entered S-phase was counted and cells

followed by a washing step and change to growth medium without the protein/peptide. Confocal microscopy of live cells was started immediately and cells were returned to the incubator between time points, which are indicated. Representative images and time points are shown. A) Uptake of 2.5 μM TAT fusion protein TAT-Cre (rhodamine-labeled) in living mouse myoblasts. After application of TAT-Cre, internalization started throughout the plasma membrane in the form of vesicles. The next day vesicles containing fluorescent TAT-Cre accumulated in the cytoplasm. B) Diffused and vesicular distribution of the TAT-HA2 peptide (rhodamine-labeled, 5 μM final concentration) soon and a long time after application. C) Simultaneous application of 2.5 μM TAT-Cre protein (Alexa Fluor 633-labeled; 1.7 label to protein ratio) and 5 μM TAT-HA2 peptide (rhodamine-labeled) on living cells resulted in prominent vesicular uptake of the protein into the cytoplasm, whereas the TAT-HA2 peptide also displays a diffuse distribution in cytoplasm and nucleoplasm, and accumulation in nucleoli. The fluorescent fusions colocalize in the majority of vesicles. Nucleoli are indicated by arrowheads. Scale bar = 10 μm . D) Analysis of Cre recombinase activity in TAT-Cre-treated reporter cells. 3T3-FDR1.2 reporter cells contain a loxP-flanked HcRed gene, followed by a nonexpressed GFP gene. TAT-Cre treatment induces recombination of the reporter gene, resulting in a shift from red to green fluorescence (scheme). Untreated control cells do not exhibit green fluorescence. Cells were incubated with 2 μM TAT-Cre for 3 h and analyzed by fluorescence microscopy 24 h later. Scale bar = 50 μm .

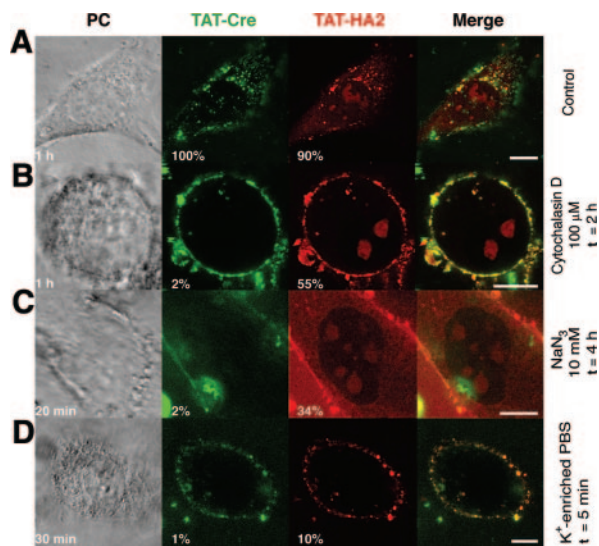


Figure 2. Different mode of uptake of proteins and peptides fused to TAT in living cells. Simultaneous incubation of living mouse myoblasts with 2.5 μM TAT-Cre and 5 μM TAT-HA2 was as shown in Fig. 2C. Confocal images show representative snapshots at the indicated time points in the phase contrast image. The numbers in the images reflect the overall percentage of cells showing intracellular vesicles for the TAT fusion protein and the nucleolar signal for the TAT-HA2 peptide. Substances at the concentrations indicated were preincubated with the cells before addition of the TAT fusions for the indicated time (t) and kept in the culture medium or buffer throughout the experiment. A) Control C2C12 mouse myoblasts treated with the TAT-containing protein and peptide mixture showed internalization in 100% and 90% of the cells, respectively. B) Preincubation of the cells with 100 μM of the F-actin elongation inhibitor cytochalasin D blocked protein uptake completely, but the peptide still transduced into the cells. C) ATP depletion with 10 mM sodium azide reduced entry of both species, albeit a third of the cells still took up the peptide. D) 5 min incubation of the cells in sodium-deficient, iso-osmolar PBS strongly reduced peptide transduction and blocked protein uptake. t = preincubation time, scale bar = 10 μm .

were transduced with fluorescently labeled TAT-p21-PBD, TAT-Lig1-PBD, and the unspecific TAT control peptide at 20 μM concentration in PBS. 10 min later the solutions were aspirated, and the cells were washed twice with medium and kept in growth medium thereafter. The percentage of cells in S-phase was determined directly from the subnuclear focal pattern of GFP-PCNA by counting 10 fields of view at the indicated time points for each peptide. Data of three independent experiments were evaluated.

Microscopy, image acquisition, and analysis

Live cell microscopy was performed with a Zeiss LSM 510 Meta confocal setup mounted on an Axiovert 200 M inverted microscope using a 63 \times phase contrast plan apochromat oil objective NA1.4. For all acquisition settings, the main beam splitter was HFT UV/488/543/633. The parameters specific for each fluorochrome were: FITC, excited at 488 nm light, detected with a 500-530 nm bandpass (BP) filter; TAMRA or rhodamine excited with 543 nm, detected with 565-615 BP and Cy5 or Alexa633 excited at 633 nm and detected with a 650 nm longpass filter.

Image acquisition was done sequentially to minimize cross-talk between the fluorophores. Phase contrast images were

recorded simultaneously with FITC/GFP fluorescence in the transmission channel. Fluorescence recovery after bleaching (FRAP) experiments (Fig. 3) was performed on a Zeiss LSM 5 Live confocal microscope with 100% power of a 75 mW DPSS 532 nm laser. The bleaching was performed in a stripe for 0.44 s, followed by a time series with 400 images recorded at 20 frames per second. Using the Zeiss LSM 510 software version 3.2, the mean fluorescence intensity in the bleached nucleoli and cytoplasm was determined over the time course and averaged for 10 cells. Fluorescence intensity was normalized to zero at the start of recovery and to one at equilibrium to directly compare the curves for both subcellular regions. The FRAP curves were generated with Origin 7 software.

RESULTS

Direct comparison of TAT-mediated peptide and protein uptake in living cells

To study the characteristics of TAT-mediated introduction of globular proteins into living cells, the rhodamine-labeled fusion protein R-TAT-Cre consisting of the CPP TAT moiety and the site-specific Cre recombinase of bacteriophage P1 (23) was applied onto C2C12 mouse myoblasts. As soon as the fluorescent solution was washed off (after 10 min of incubation), fluorescent vesicles emerging from the intracellular side of the plasma membrane were detectable by confocal microscopy (Fig. 2A, upper panel). After additional overnight cultivation, all cells showed a substantial amount of internalized protein stored in vesicles, but release of the protein from the vesicles could not be detected by this method (Fig. 2A, lower panel). Other recombinant proteins showed identical trapping in cytoplasmic vesicles (data not shown) independent of 1) which short basic CPP they were fused to, 2) the fluorophore they were conjugated to, and 3) their known subcellular localization. For instance the nuclear protein His-PTD₄-PCNA (Atto 633-labeled) as well as the nuclear and cytoplasmic protein His-TAT-MK2 (Cy5-labeled) could only be detected inside cytoplasmic vesicles after internalization, and refused to localize at their targets during an observation period of up to 48 h. Proteins lacking a transduction domain could also be internalized in the same manner but the efficiency of internalization was shown to be much lower (23). TAT-Cre was also tested at concentrations between 0.1 and 10 μM with no difference in the uptake behavior (data not shown).

A recent report proposed that the uptake of proteins fused to TAT belongs to the class of rapid lipid raft-mediated macropinocytosis and that the protein could be released from macropinosomes by cotransduction of the fusogenic peptide TAT-HA2 (17). We therefore used TAT-HA2 (Table 1) to 1) work out the characteristics of TAT-mediated peptide (<50 amino acids; ref. 28) transduction and 2) try and liberate the TAT fusion protein trapped into vesicles. Compared to the internalization of proteins, uptake of the TAT-HA2 peptide occurred on a quite different time scale and also showed dissimilarities in its subcellular localization. During the first 3–5 min of incubation with the peptide

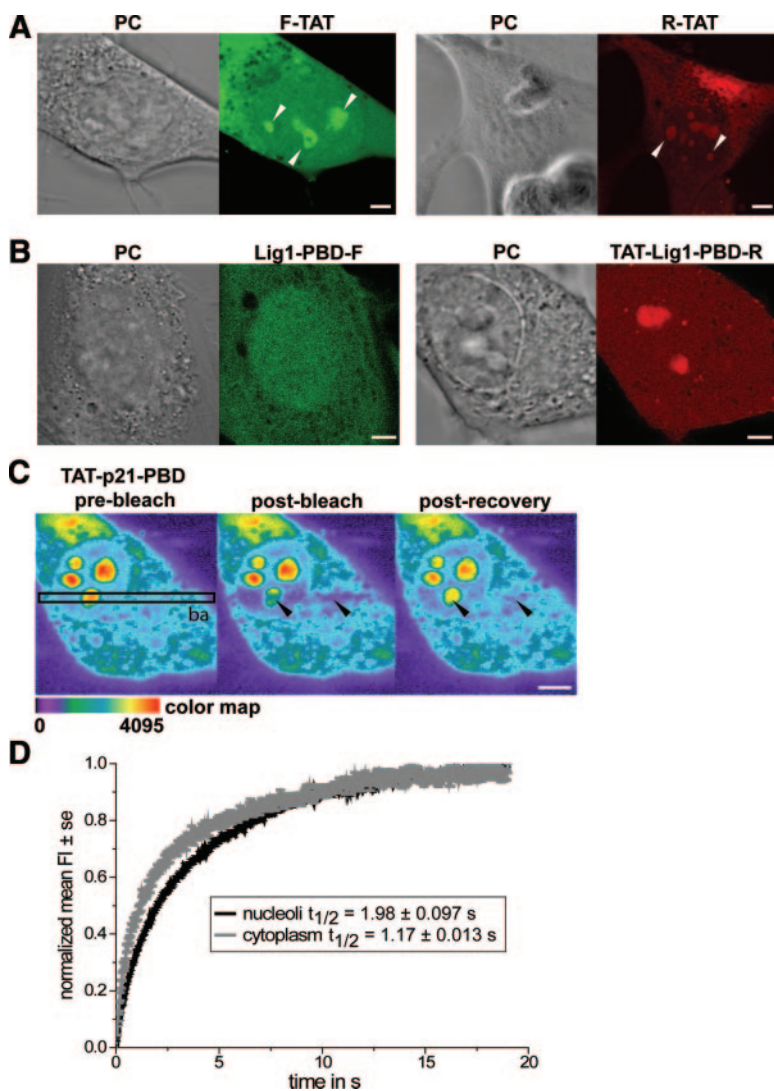


Figure 3. Subcellular localization and intracellular mobility of TAT peptides. *A*) FITC- and rhodamine-labeled TAT peptides (F-TAT 1 μ M, R-TAT 1 μ M) applied to mouse myoblasts were rapidly internalized and accumulated in the nucleoli (white arrowheads). The fluorescent label has no influence on peptide distribution. *B*) In contrast, the non-TAT-containing peptide Lig1-PBD (FITC-labeled) delivered by bead loading showed a homogeneous distribution in nucleus and cytoplasm whereas the addition of the TAT sequence in TAT-Lig1-PBD (rhodamine-labeled) again led to nucleolar accumulation. *C*) Mouse myoblasts were transduced with 20 μ M of TAMRA-labeled TAT-p21-PBD for 10 min, washed, then incubated in growth medium. The FRAP experiment was performed by bleaching a stripe (ba) encompassing one nucleolus and a part of the cytoplasm as seen in the prebleach image. After bleaching, a time series was recorded at a time resolution of 20 frames/second over 20 s. False color images depicting the fluorescence intensity distribution as color map (red denotes highest intensity) of one photobleached cell are shown. The black arrowheads point to the bleached nucleolus and cytoplasmic regions in the first image after the bleaching process (postbleach) and after full fluorescence recovery (postrecovery). *D*) Curves represent the normalized mean fluorescence intensity of the fluorescence recovery in the nucleoli and cytoplasm averaged for 10 measurements. Albeit accumulated in the nucleoli, the TAT-p21-PBD peptide was highly mobile with a half-time of recovery of 1.98 ± 0.097 s. In the cytoplasm, the half-time of recovery is faster (1.17 ± 0.013 s). Scale bar = 5 μ m.

solution, fluorescence signals had already become visible in the nucleoli; after exchange of the fluorescent solution against medium, a diffuse distribution throughout the cell, with accumulation in the nucleoli, could be detected (Fig. 2B, upper panel, arrowheads; see also supplemental movie) in addition to a few developing vesicles adjacent to the membranes. Over longer periods of observation, the diffuse population of the peptide in the cytoplasm, nucleoplasm, and nucleoli became markedly weaker, and in most of the cells vanished overnight. In stark contrast, the peptide-containing cytoplasmic vesicles seemed to be unaffected and their number increased overnight, resulting in a vesicular ring concentrated around the nucleus (Fig. 2B, lower panel). The diffusely distributed fraction of the transduced peptide was detected in $\sim 90\%$ of the cells (Table 1) whereas after overnight incubation all cells showed peptide uptake into vesicles. The loss of diffusely distributed fluorescent peptide in the cytoplasm and nuclei overnight cannot be just a consequence of instability of the fluorophore/peptide in the cell since 1) a rhodamine-labeled antibody (Ab) persisted inside cells for > 24 h (data not shown) and 2)

the fluorescently labeled peptide TAT-HA2 is composed of protease-resistant D-amino acids.

To directly compare the mode and kinetics of uptake of TAT peptides and globular proteins fused to TAT into cells and determine whether TAT-HA2 could drive release of the protein stored in macropinosomes, the Alexa Fluor 633-labeled TAT-Cre protein and the rhodamine-labeled TAT-HA2 peptide were applied simultaneously to living cells. The short- and long-term uptake characteristics for both species remained mostly unchanged (Fig. 2C). Detectable TAT fusion protein was restricted to cytoplasmic vesicles whereas the TAT-HA2 peptide, besides being trapped into vesicles, was rapidly distributed throughout the entire cell. TAT-HA2 and TAT-Cre colocalized in the majority of cytoplasmic vesicles (Fig. 2C, yellow color in merged images). Although both species intermingled substantially, a release of the TAT fusion protein from macropinosomes and entry into the nucleus could not be detected by this method. To test the presence of a low level of TAT-Cre within the nucleus, we used a far more sensitive reporter assay based on Cre-mediated recombination. Since site-specific recombination provides a stable and unambigu-

ous read-out for protein transduction (23, 29–31), we used a NIH-3T3 Cre reporter cell line containing a stably integrated gene cassette consisting of a constitutively expressed HcRed gene, followed by a nonexpressed GFP gene. Upon Cre recombinase-mediated site-specific recombination, excision of the HcRed gene takes place with concomitant expression of the GFP gene (Fig. 2D; L. Nolden and F. Edenhofer, personal communication). Using this more sensitive assay, several cells within the culture exhibited GFP expression upon incubation with TAT-Cre overnight (Fig 2D). These data indicate that a low level of TAT-Cre below the detection range of confocal microscopy was biologically available and could exert its enzymatic activity.

Different mode of entry of proteins and peptides fused to TAT in living cells

To test whether TAT fusion proteins and TAT-containing peptides use different routes of entry and can, as a result, be affected differently in their uptake by treatment with inhibitors, mouse myoblasts were preincubated with inhibitors or buffers, followed by simultaneous application of TAT-Cre and TAT-HA2 (as in Fig. 2C). Subsequently, cells were washed twice and kept in the indicated buffer or medium with constant inhibitor concentration throughout the entire experiment.

Endocytosis requires the formation and migration of vesicles along the cytoskeleton. Therefore, constant concentrations of the F-actin depolymerizing drug cytochalasin D should delay or block internalization of the endocytosed TAT constructs at the membrane level (32, 33). After cytochalasin D treatment, the TAT fusion protein and TAT-HA2 showed strong membrane association, but the diffused fraction of the TAT-HA2 peptide was still detectable inside the cells in nucleoli, albeit the transduction efficiency (as scored by the percentage of cells showing intracellular fluorescence) was reduced to half. All vesicular uptake was abolished (Fig. 1B). Despite the round appearance of the cells indicative of the disruptive effect of the drug on the actin cytoskeleton, the membrane integrity was not decreased as assayed by Trypan blue exclusion (data not shown).

Endocytosis is an energy-consuming process and is therefore blocked by the metabolic inhibitor sodium azide. Accordingly, treatment with 10 mM sodium azide resulted in almost complete inhibition of the internalization of the TAT fusion protein (scored by the absence of intracellular vesicles), whereas the diffused population of the TAT-HA2 was still detected in about one-third of the cells (Fig. 1C).

A recent report proposed that synthetic guanidinium-rich molecules traverse biological membranes by formation of lipophilic ion pairs between the guanidinium groups and abundant phosphate, sulfate, and carboxylate functions on the membrane surface, allowing cell entry by diffusion along the membrane potential and subsequent release of the positively charged CPP into the cytoplasm (5, 10). The directionality of

this process is achieved by the membrane potential and the latter can be efficiently reduced by addition of an isotonic buffer with potassium concentrations equivalent to those found intracellularly (34, 35). We tested this hypothesis by preincubating the cells for 5 min with potassium-enriched, isotonic PBS and adding the peptide/protein solution in the same buffer. This treatment abolished the vesicular internalization of both TAT species. Furthermore, it resulted in strong inhibition of the uptake mode responsible for the intracellularly diffused fraction of TAT-HA2 (Fig. 1D). In summary, in contrast to TAT fused to globular proteins, TAT fusion peptides transduce into cells by a different and very rapid mode that is dependent on the plasma membrane potential. We therefore further investigated the transduction potential and biological applicability of TAT fusion peptides.

Uptake and intracellular availability of TAT-containing peptides

In the first minutes of incubation, the TAT-HA2 peptide flooded into living cells and accumulated in nucleoli; later it was also localized in cytoplasmic vesicles (Fig. 2B, C). To test whether these uptake characteristics were influenced by the HA2 moiety or instead were a general feature of TAT-mediated peptide internalization, several TAT peptide complexes were analyzed for their transduction behavior and intracellular distribution after internalization. Table 1 summarizes the peptides and their respective transduction efficiencies determined, as earlier, by counting the percentage of cells showing intracellular diffused fluorescence upon 10 min incubation with the indicated peptide concentrations and analyzed by confocal microscopy of living cells. The most efficient peptide was the 11 amino acid TAT peptide covalently linked to either a FITC (F) or a rhodamine (R) fluorophore, which was transduced into 90% of all cells at 1 μ M concentration within the first 3 min of observation. The fluorescent signal appeared diffused in the cytoplasm and nucleoplasm and showed strong accumulation of the labeled peptide in nucleoli (Fig. 3A). To test whether the nucleoli accumulation was due to the TAT moiety, we used non-TAT-containing peptides (Lig1-PBD in Fig. 3B and NLS-biotin peptide complexed with streptavidin-Cy5 [data not shown]) and delivered them into the cytoplasm using either bead loading or microinjection. Both peptides were stable intracellularly and able to enter the nucleus, but were not accumulated in the nucleoli (Fig. 3B and data not shown). The same Lig1-PBD peptide fused to TAT (TAT-Lig1-PBD) transduced into cells and again showed nucleolar localization (Fig 3B), indicating that the nucleolar localization is dependent on the TAT characteristics. We investigated other reported CPPs—namely, PTD4 (36)—which showed only detectable uptake (Table 1) at very high concentrations (400 μ M). This suggests that nucleolar association is mediated by the high concentration of positive charges due to arginine and lysine residues.

Since TAT fusion peptides exhibited accumulation in the nucleolar compartment whereas the cargo peptide or protein may perform its function in a different subcellular compartment, we tested the overall bioavailability of cargoes connected to TAT by directly measuring the mobility in living cells using fluorescence photobleaching analysis. Cells transduced with a TAT-containing peptide (TAT-p21-PBD, Table 1) were imaged, and a rectangular region was selected to include one nucleolus and a stripe of cytoplasm. The peptide fluorescence in this stripe was subsequently photobleached with a high intensity laser beam, and redistribution of fluorescence was measured over time until full equilibrium was regained. The peptide intensity distribution before (prebleach), immediately after (postbleach), and at full recovery (postrecovery) is shown in representative false color images in Fig. 3C. The recovery of fluorescence in the bleached region indicates the mobility of peptides from unbleached cellular regions into the bleached area, and therefore is a direct measure of peptide mobility in the living cells. The kinetics of recovery (Fig. 3D) indicated that the peptides, although concentrated in the nucleoli, were mobile with a half-time of recovery of 1.98 and 1.17 s in the nucleoli and cytoplasm respectively. This kinetic difference between nucleoli and cytoplasm suggests binding of the TAT-PBD-p21 within the nucleoli. The high intracellular mobility of the TAT peptides raises the possibility of achieving successful biological effects despite the unfavorable subcellular accumulation.

Cell cycle inhibition by transduced PCNA binding peptides

To directly test whether the transduced TAT peptides in view of their high mobility could be effective in reaching their intracellular targets and exerting a biological effect, we used fusions of TAT with two different peptides comprising the proliferating cell nuclear antigen (PCNA) binding domain (PBD) of p21^{WAF/CIP} and DNA Ligase 1 (Table 1). These two peptides have been shown to bind to PCNA (20, 22). We reasoned that since several PCNA interacting proteins required for S-phase progression utilize the same binding interface on the surface of PCNA, competition for binding should ensue and inhibition of cell cycle progression would be expected. Mouse myoblasts stably expressing the cell cycle progression marker GFP-PCNA (26) were synchronized in the G₁ phase of the cell cycle by mitotic shake off. After becoming adherent, the G₁ synchronized cells were incubated for 10 min with either of these two TAT-PBD peptides as well as a control TAT fusion peptide (37). After washing, peptide uptake efficiency was controlled for by counting the percentage of cells showing intracellular peptide fluorescent signal as before. At different times thereafter, the ability of cells to progress into S-phase was determined by counting the number of S-phase cells scored by the characteristic focal GFP-PCNA subnuclear distribution pattern (see green subnuclear signal in the examples

shown in images in Fig. 4 and ref. 26) directly under the fluorescent microscope. The results of this live cell cycle assay are summarized in Fig. 4. While 70% control cells and cells incubated with TAT control peptide were in S-phase 6 h after peptide incubation, only ~40% TAT-PBD-treated cells entered S-phase within the same time. This inhibition is even more noteworthy if one considers that the peptides were incubated with the cells for only 10 min, after which they were washed away. Toxic effects were not detected by either the Trypan blue exclusion test or by changes in cell morphology. These data demonstrate that both TAT-PBD peptides were bioactive and capable of decelerating cell cycle progression despite the short incubation time and their accumulation in the nucleolus (see also red fluorescence peptide signal in the images in Fig. 4).

DISCUSSION

Although it is generally agreed that the first step in the internalization process of CPP-mediated transduction is the strong ionic interaction between the cationic CPP and negatively charged plasma membrane constituents (6, 15, 38), subsequent steps for CPP-induced cell entry differ in the recent literature and range from endocytic (15, 19) to a rapid and energy-independent process (6, 12). Most studies so far have used fixed cell analysis, which has been shown to result in artificial internaliza-

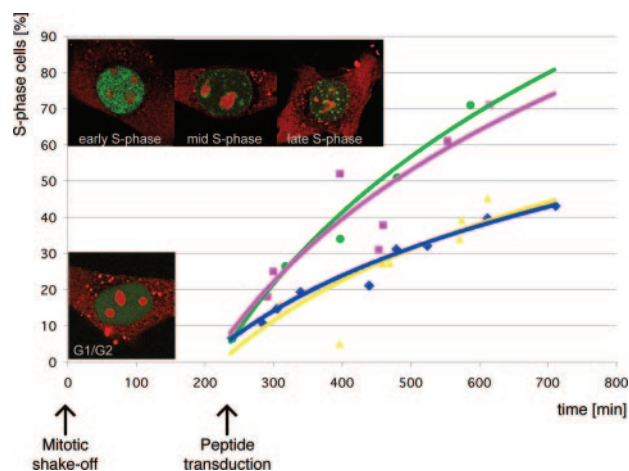


Figure 4. Effect of transduced PBD-containing TAT peptides on cell cycle progression. After mitotic shake-off, GFP-PCNA-expressing mouse myoblasts were allowed to attach and were incubated with different peptides (20 μ M) for 10 min, followed by washing and a change to growth medium. The percentage of S-phase cells was determined at various time points by the subnuclear replication foci pattern of GFP-PCNA. Representative confocal microscopy images of mouse myoblasts transduced with the TAMRA-labeled TAT-p21-PBD peptide (red) show either a diffused distribution of GFP-PCNA (green) in the nucleus, indicating G₁- or G₂-phase or focal GFP-PCNA labeling of replication foci during early, mid and late S-phase. Data points of three independent experiments were fitted logarithmically. Control cells, pink squares; TAT control peptide, green spheres; TAT-Lig1-PBD peptide, yellow triangles; and TAT-p21-PBD peptide, blue diamonds.

tion of CPP-containing constructs. In this work we used exclusively live cell analysis and tested whether the mode of entry is dependent on the cargo connected to the CPP and what the fate and bioavailability of the transduced peptides is.

By directly comparing the uptake of TAT connected to peptides and globular proteins into living cells, we found that the mechanism of entry depends on the size of the cargo fused to TAT. The major fraction of TAT-containing proteins or peptides was taken up into living cells by distinct modes, with the proteins mostly ending up in cytoplasmic vesicles and the peptides distributing throughout the cell and accumulating in the nucleoli (Fig. 2).

The vesicular storage inside the cytoplasm was a general feature of different recombinant proteins fused to a CPP and was independent of protein function, CPP (data not shown), and fluorescent label (Fig. 2A, C). A small population of TAT fusion protein reached the cytosol and nucleus via a different pathway or leaked out from the vesicles, as we detected Cre recombination activity in the nuclei using an extremely sensitive and unambiguous reporter assay for TAT-Cre. This fraction of bioavailable TAT-Cre was not high enough, however, to be detected by direct confocal microscopy of the labeled TAT-Cre protein whereas the population trapped in vesicles was easily detectable. Furthermore, cotransduction of the fusogenic peptide TAT-HA2 (17) did not substantially increase the release of the different TAT fusion proteins from cytoplasmic vesicles as assayed by live cell confocal microscopy (Fig. 2C).

Unlike CPP fusion proteins, TAT fusion peptides could be seen diffusely distributed throughout the cell and concentrated in nucleoli (Fig. 2 and Table 1). Uptake occurred rapidly within 3–5 min after application of the TAT construct on living cells. Upon longer observation times, the diffusely distributed fraction of the TAT peptides disappeared and cytoplasmic vesicles containing the peptides became apparent, suggesting that the peptides were either redistributed or underwent an additional vesicular uptake.

In addition to different uptake kinetics and localization after internalization of proteins and peptides fused to CPPs, inhibitors of endocytosis efficiently blocked the vesicular uptake of both species while having a minor effect on the TAT peptide transduction (Fig. 1), indicating that the latter does not depend on vesicle formation and/or traffic along the cytoskeleton. In fact, the only treatment capable of blocking not only the vesicular uptake of CPP-containing proteins and peptides, but also the rapid translocation of TAT peptides leading to a diffuse intracellular distribution, was incubation of the cells with a sodium-deficient iso-osmolar buffer (Fig. 1), indicating an alternative distinct cellular entry pathway based on membrane potential.

To understand which properties of cargoes fused to TAT allow the rapid membrane transduction, we compared the cellular entry of various TAT-containing constructs (Table 1). Fluorescently labeled TAT had already appeared inside the nucleoli of 90% of living

cells at a concentration of 1 μM . The uptake efficiencies were decreased for TAT fusion peptides. By comparison, differences in the overall pI of TAT due to the addition of a cargo resulted only in minor effects on transduction efficiencies, whereas the amino acid composition of the CPP itself seemed to be more important. For instance, PTD₄ containing three arginines transduced into living cells only at concentrations of >400 μM whereas TAT peptides with eight positive charges (six of them arginines) transduced quite efficiently in a range of 0.1–10 μM (Table 1). Most transduction efficiencies were tested for the CPP TAT at concentrations of 10 μM and resulted in comparable high percentages of transduced cells. However, differences for individual peptides were found to be dependent on the concentration used; for instance, the TAT-HA2 peptide was already diffusely distributed inside cells at a concentration of 0.1 μM , whereas for TAT-p21-PBD uptake was restricted to endocytosis below a concentration of 7.5 μM , and only above 7.5 μM did the peptide enter rapidly and appear in the nucleoli (Table 1). The existence of such a concentration threshold can also explain conflicting reports assigning CPP-mediated membrane translocation to endocytosis (19, 39) or to an unknown mechanism, resulting in a homogeneous distribution in the whole cell (7). Another parameter that should be taken into account is the stability of the transducible peptides themselves since it was shown that CPP peptides could be degraded by extra- and intracellular proteases (40). However, we have not observed dramatic differences in the transduction efficiencies between TAT-HA2 consisting of D-amino acids and other potentially degradable peptides consisting of L-amino acids at comparable concentrations (Table 1).

The TAT-containing peptides exhibited a strong affinity to the nucleolar compartment, with a lower steady-state concentration in the rest of the cell. Alternatively, their enrichment in the nucleoli could be due to a higher viscosity in this subnuclear compartment. However, our fluorescence photobleaching results (Fig. 3) revealed that despite their accumulation in the nucleolus, TAT peptides were mobile and able to reach their targets in the nucleus and cytoplasm. Measurements of protein dynamics in the cell nucleus showed half recovery times of <3 s, and so the peptide dynamics measured for TAT-p21-PBD in nucleoli and cytoplasm (<2 s) can be considered to be similar (41). As a direct test of their bioavailability, we investigated the cell cycle effects of TAT fusion to PBD peptides. PCNA forms a sliding clamp around DNA and plays a central role in DNA replication (reviewed in ref. 42). Multiple factors required for DNA synthesis and cell cycle progression bind PCNA (20) via a consensus PBD Qxx(M/L/I)xxF(Y/F) (43). We fused two different PBD peptides to TAT and tested their effect on cell cycle progression using a novel live cell cycle progression assay. In fact, incubation of the cells with both peptides for as little as 10 min substantially inhibited cell cycle progression (Fig. 4). These data clearly showed that, albeit accumulated in nucleoli, the peptides are fully

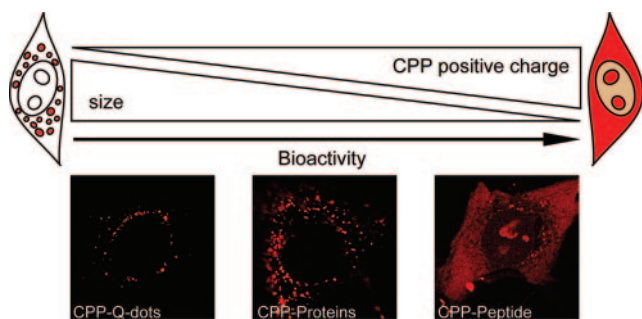


Figure 5. Influence of molecule size and charge on cellular uptake through endocytosis vs. transduction. Cargoes fused to CPPs follow different routes of entry into living mammalian cells. The complexes or fusions of CPPs with large 20 nm diameter Quantum Dots down to globular proteins are mainly endocytosed and remain trapped in cytoplasmic vesicles. Small, nonglobular peptides fused to CPPs are to a certain extent also endocytosed, but in addition are taken up into living cells by membrane transduction; inside the cells they are highly mobile and capable of reaching any subcellular compartment. Thus, transduction of peptides leads to rapid internalization in a bioactive manner whereas globular particles are largely trapped inside vesicles. The mode of uptake is influenced by the charge of the CPP and the size of the cargo connected to it.

able to reach their biological targets elsewhere in the cell and exert a biological effect.

In summary, our data indicate that the translocation of TAT-containing constructs through biomembranes takes place with high efficiency, but at least two functionally distinct mechanisms are involved. Complexes with a globular structure like TAT fused to Q-dots (Fig. 5) or TAT fusion proteins seem to be mostly restricted in their uptake to an endocytic mechanism that is associated with trapping in cytoplasmic vesicles. A minor fraction of internalized TAT fusion proteins, undetectable by confocal microscopy but sufficient to induce enzymatic activity, seems to escape vesicles in the cells. Besides being endocytosed, TAT-containing peptides have the ability to enter living cells by a different pathway. The exact underlying mechanism for this rapid translocation is unknown and could be explained by transient membrane perturbations (14) or lipophilic ion pair diffusion along the membrane potential (5, 10). In general, increasing positive charge of the CPP itself and decreasing size of the cargo fused to the CPP allows rapid internalization to occur in addition to the slow process of adsorptive endocytosis (Fig. 5). The latter implies that CPP-mediated uptake of globular proteins is restricted to cell types capable of endocytosis. CPP-containing peptides can rapidly transduce all cell types tested and, despite their high affinity to the nucleolus, transduced peptides have access to all intracellular compartments, thus making them an ideal tool for therapeutic applications. **[F]**

We thank A. Krella, P. Domaing, and M. Peitz for their participation at earlier stages of this project. We are indebted to R. Kettritz (Franz Volhard Clinic, Berlin) and U. Kubitschek (University of Bonn) for providing some of the pep-

tides used, M. Gaestel (University of Hannover) for the gift of expression plasmids for MK2, and H. Leonhardt (Ludwig Maximilians University, Munich) for advice throughout this work. We thank members of the Stem Cell Engineering Group (University of Bonn) for support and valuable discussions. This work was supported in part by the Max Delbrueck Center and by grants from the Deutsche Forschungsgemeinschaft and the Volkswagen Foundation (M.C.C.) as well as by grants from the Stem Cell Network North Rhine Westphalia, the European Union and the Volkswagen Foundation (F.E.).

REFERENCES

- Dietz, G. P., and Bdeltahr, M. (2004) Delivery of bioactive molecules into the cell: the Trojan horse approach. *Mol. Cell Neurosci.* **27**, 85–131
- Richard, J. P., Melikov, K., Vives, E., Ramos, C., Verbeure, B., Gait, M. J., Chernomordik, L. V., and Lebleu, B. (2003) Cell-penetrating peptides. A reevaluation of the mechanism of cellular uptake. *J. Biol. Chem.* **278**, 585–590
- Cardoso, M. C., and Leonhardt, H. (2002) Protein transduction: a novel tool for tissue regeneration. *J. Biol. Chem.* **383**, 1593–1599
- Vives, E., Brodin, P., and Lebleu, B. (1997) A truncated HIV-1 Tat protein basic domain rapidly translocates through the plasma membrane and accumulates in the cell nucleus. *J. Biol. Chem.* **272**, 16010–16017
- Dom, G., Shaw-Jackson, C., Matis, C., Bouffieux, O., Picard, J. J., Prochiantz, A., Mingeot-Leclercq, M. P., Brasseur, R., and Rezsöházy, R. (2003) Cellular uptake of Antennapedia Penetratin peptides is a two-step process in which phase transfer precedes a tryptophan-dependent translocation. *Nucleic Acids Res.* **31**, 556–561
- Mai, J. C., Shen, H., Watkins, S. C., Cheng, T., and Robbins, P. D. (2002) Efficiency of protein transduction is cell type-dependent and is enhanced by dextran sulfate. *J. Biol. Chem.* **277**, 30208–30218
- Ziegler, A., Blatter, X. L., Seelig, A., and Seelig, J. (2003) Protein transduction domains of HIV-1 and SIV TAT interact with charged lipid vesicles. Binding mechanism and thermodynamic analysis. *Biochemistry* **42**, 9185–9194
- Mitchell, D. J., Kim, D. T., Steinman, L., Fathman, C. G., and Rothbard, J. B. (2000) Polyarginine enters cells more efficiently than other polycationic homopolymers. *J. Pept. Res.* **56**, 318–325
- Thoren, P. E., Persson, D., Isakson, P., Gokso, M., Onfelt, A., and Norden, B. (2003) Uptake of analogs of penetratin, Tat(48–60) and oligoarginine in live cells. *Biochem. Biophys. Res. Commun.* **307**, 100–107
- Rothbard, J. B., Jessop, T. C., and Wender, P. A. (2005) Adaptive translocation: the role of hydrogen bonding and membrane potential in the uptake of guanidinium-rich transporters into cells. *Adv. Drug Deliv. Rev.* **57**, 495–504
- Scheller, A., Wiesner, B., Melzig, M., Bienert, M., and Oehlke, J. (2000) Evidence for an amphipathicity independent cellular uptake of amphipathic cell-penetrating peptides. *Eur. J. Biochem.* **267**, 6043–6050
- Ziegler, A., Nervi, P., Durrenberger, M., and Seelig, J. (2005) The cationic cell-penetrating peptide CPP(TAT) derived from the HIV-1 protein TAT is rapidly transported into living fibroblasts: optical, biophysical, and metabolic evidence. *Biochemistry* **44**, 138–148
- Futaki, S., Suzuki, T., Ohashi, W., Yagami, T., Tanaka, S., Ueda, K., and Sugiura, Y. (2001) Arginine-rich peptides. An abundant source of membrane-permeable peptides having potential as carriers for intracellular protein delivery. *J. Biol. Chem.* **276**, 5836–5840
- Prochiantz, A. (2000) Messenger proteins: homeoproteins, TAT and others. *Curr. Opin. Cell Biol.* **12**, 400–406
- Vives, E. (2003) Cellular uptake [correction of utake] of the Tat peptide: an endocytosis mechanism following ionic interactions. *J. Mol. Recognit.* **16**, 265–271
- Fittipaldi, A., Ferrari, A., Zoppe, M., Arcangeli, C., Pellegrini, V., Beltram, F., and Giacca, M. (2003) Cell membrane lipid rafts

- mediate caveolar endocytosis of HIV-1 Tat fusion proteins. *J. Biol. Chem.* **278**, 34141–34149
17. Wadia, J. S., Stan, R. V., and Dowdy, S. F. (2004) Transducible TAT-HA fusogenic peptide enhances escape of TAT-fusion proteins after lipid raft macropinocytosis. *Nat. Med.* **10**, 310–315
 18. Caron, N. J., Quenneville, S. P., and Tremblay, J. P. (2004) Endosome disruption enhances the functional nuclear delivery of Tat-fusion proteins. *Biochem. Biophys. Res. Commun.* **319**, 12–20
 19. Kaplan, I. M., Wadia, J. S., and Dowdy, S. F. (2005) Cationic TAT peptide transduction domain enters cells by macropinocytosis. *J. Control Release* **102**, 247–253
 20. Gulbis, J. M., Kelman, Z., Hurwitz, J., O'Donnell, M., and Kuriyan, J. (1996) Structure of the C-terminal region of p21 (WAF1/CIP1) complexed with human PCNA. *Cell* **87**, 297–306
 21. Cardoso, M. C., Joseph, C., Rahn, H. P., Reusch, R., Nadal-Ginard, B., and Leonhardt, H. (1997) Mapping and use of a sequence that targets DNA ligase I to sites of DNA replication in vivo. *J. Cell Biol.* **139**, 579–587
 22. Montecucco, A., Rossi, R., Levin, D. S., Gary, R., Park, M. S., Motycka, T. A., Ciarrocchi, G., Villa, A., Biamonti, G., and Tomkinson, A. E. (1998) DNA ligase I is recruited to sites of DNA replication by an interaction with proliferating cell nuclear antigen: identification of a common targeting mechanism for the assembly of replication factories. *EMBO J.* **17**, 3786–3795
 23. Peitz, M., Pfannkuche, K., Rajewsky, K., and Edenhofer, F. (2002) Ability of the hydrophobic FGF and basic TAT peptides to promote cellular uptake of recombinant Cre recombinase: a tool for efficient genetic engineering of mammalian genomes. *Proc. Natl. Acad. Sci. U. S. A.* **99**, 4489–4494
 24. Caron, N. J., Torrente, Y., Camirand, G., Bujold, M., Chapdelaine, P., Leriche, K., Bresolin, N., and Tremblay, J. P. (2001) Intracellular delivery of a Tat-eGFP fusion protein into muscle cells. *Mol. Ther.* **3**, 310–318
 25. Cardoso, M. C., Leonhardt, H., and Nadal-Ginard, B. (1993) Reversal of terminal differentiation and control of DNA replication: cyclin A and Cdk2 specifically localize at subnuclear sites of DNA replication. *Cell* **74**, 979–992
 26. Leonhardt, H., Rahn, H. P., Weinzierl, P., Sporbert, A., Cremer, T., Zink, D., and Cardoso, M. C. (2000) Dynamics of DNA replication factories in living cells. *J. Cell Biol.* **149**, 271–280
 27. Nolden, L., Edenhofer, F., Haupt, S., Koch, P., Wunderlich, F. T., Siemen, H., and Brustle, O. (2006) Site specific recombination in human ES cells induced by cell permeable Cre recombinase. *Nat. Methods* In press
 28. Seewald, N., and Jakubke, H.-D. (2002) *Peptides: Chemistry and Biology*, Wiley-VCH, Weinheim, Germany
 29. Jo, D., Nashabi, A., Doxsee, C., Lin, Q., Unutmaz, D., Chen, J., and Ruley, H. E. (2001) Epigenetic regulation of gene structure and function with a cell-permeable Cre recombinase. *Nat. Biotechnol.* **19**, 929–933
 30. Joshi, S. K., Hashimoto, K., and Koni, P. A. (2002) Induced DNA recombination by Cre recombinase protein transduction. *Genesis* **33**, 48–54
 31. Will, E., Klump, H., Heffner, N., Schwieger, M., Schiedlmeier, B., Ostertag, W., Baum, C., and Stocking, C. (2002) Unmodified Cre recombinase crosses the membrane. *Nucleic Acids Res.* **30**, e59
 32. Goddette, D. W., and Frieden, C. (1986) The kinetics of cytochalasin D binding to monomeric actin. *J. Biol. Chem.* **261**, 15970–15973
 33. Flanagan, M. D., and Lin, S. (1980) Cytochalasins block actin filament elongation by binding to high affinity sites associated with F-actin. *J. Biol. Chem.* **255**, 835–838
 34. Aidley, D., and Stanfield, P. (1996) *Ion Channels: Molecules in Action*, Cambridge University Press, Cambridge, England
 35. Watanabe, Y., Kameoka, S., Gopalakrishnan, V., Aldape, K. D., Pan, Z. Z., Lang, F. F., and Majumder, S. (2004) Conversion of myoblasts to physiologically active neuronal phenotype. *Genes Dev.* **18**, 889–900
 36. Ho, A. (2001) Synthetic protein transduction domains: enhanced transduction potential in vitro and in vivo. *Cancer Res.* **61**, 474–475
 37. Choi, M., Rolle, S., Wellner, M., Cardoso, M. C., Scheidereit, C., Luft, F. C., and Kettritz, R. (2003) Inhibition of NF-kappaB by a TAT-NEMO binding domain peptide accelerates constitutive apoptosis and abrogates LPS-delayed neutrophil apoptosis. *Blood* **102**, 2259–2267
 38. Tyagi, M., Rusnati, M., Presta, M., and Giacca, M. (2001) Internalization of HIV-1 tat requires cell surface heparan sulfate proteoglycans. *J. Biol. Chem.* **276**, 3254–3261
 39. Vives, E., Richard, J. P., Rispal, C., and Lebleu, B. (2003) TAT peptide internalization: seeking the mechanism of entry. *Curr. Protein Pept. Sci.* **4**, 125–132
 40. Fischer, R., Kohler, K., Fotin-Mleczek, M., and Brock, R. (2004) A stepwise dissection of the intracellular fate of cationic cell-penetrating peptides. *J. Biol. Chem.* **279**, 12625–12635
 41. Phair, R. D., and Misteli, T. (2000) High mobility of proteins in the mammalian cell nucleus. *Nature* **404**, 604–609
 42. Maga, G., and Hubscher, U. (2003) Proliferating cell nuclear antigen (PCNA): a dancer with many partners. *J. Cell Sci.* **116**, 3051–3060
 43. Warbrick, E. (1998) PCNA binding through a conserved motif. *Bioessays* **20**, 195–199

Received for publication December 3, 2005.

Accepted for publication April 10, 2006.